ELSEVIER

Journal of Power Sources 53 (1995) 215–228

JOURNAL OF POWER SOURCES

Pulsed-current charging of lead/acid batteries — a possible means for overcoming premature capacity loss?

L.T. Lam *, H. Ozgun, O.V. Lim, J.A. Hamilton, L.H. Vu, D.G. Vella, D.A.J. Rand

CSIRO Division of Mineral Products, Port Melbourne, Vic. 3207, Australia

Received 22 August 1994; accepted 6 September 1994

Abstract

A pulsed-current technique is evaluated for the rapid charging of lead/acid cells that are prepared with either low-antimony or lead–calcium–tin grids. For comparative purposes, these cells are subjected to repetitive reserve-capacity cycling under either pulsed-current or conventional, invariant-current recharge. Although the latter charging is recommended by the manufacturers of the respective grids, it invokes premature capacity loss when combined with the high-rate discharge of the reserve-capacity test. Two significant benefits are found with the pulsed-current technique, namely, a reduction in recharging time by an order of magnitude (i.e., from ~10 to ~1 h), and an increase in cycle life by a factor of three to four. Temperature effects play only a minor role in prolonging battery endurance under pulsed-charging conditions. The technique also has the ability to recover the capacity of cycled cells. As expected, premature capacity loss occurs in both Pb–Sb and Pb–Ca–Sn cells cycled under invariant-current charging. The phenomenon is more acute in Pb–Ca-based cells. The decline in capacity of Pb–Sb cells is associated with a progressive change in the nature of the positive active material, i.e., from low crystallinity in the precursor material to a more defined crystallinity in the cycled mass. This behaviour reduces both the available surface area and the reactivity of the active material with the battery acid. By contrast, the capacity loss in Pb–Ca–Sn cells is related to both a progressive increase in the crystallization of the active material during cycling (i.e., development of small crystals) and to the growth of a resistive 'PbO' layer immediately adjacent to the grid member. The latter phenomenon is the more dominant. Pulsed-current charging is found to be an effective means for delaying the crystallization process in the active material, as well as for minimizing the development of the 'PbO' layer during cycling. Thus, pulsed charging offers a promising approach towards enhancing the cycle life of Pb–Sb and — more importantly — Pb–Ca–Sn cells, particularly under rapid-recharge conditions.

Keywords: Lead/acid batteries; Premature capacity loss; Pulsed-current charging

1. Introduction

There is a growing demand for the development and introduction of battery-powered, electric road vehicles (EVs) to combat air pollution in urban environments, as well as to reduce the global consumption of limited supplies of fossil fuels. At present, candidate energy-storage systems for motive-power applications include lead/acid, nickel/cadmium, nickel/metal-hydride, zinc/air, zinc/bromine, sodium/nickel-chloride and rechargeable lithium batteries. Among these, the lead/acid battery has clear advantages. The battery has a proud history of service (e.g., traction units have been used for decades to power fork-lift trucks, golf carts, wheelchairs, mining locomotives and submarines), a well-established network of manufacturers and distributors, a competitive cost, and efficient recycling facilities. For such reasons, lead/acid technology is considered widely to be the most effective, reliable, safe and affordable power source for the near-term EV market.

To provide traffic-compatible EVs, lead/acid traction batteries (or, indeed, any battery technology), must have high energy- and power-to-weight ratios, good service life, and low cost. For example, the targets set by the Advanced Lead-Acid Battery Consortium are 50 Wh kg^{-1} (*C*/3 rate), 150 W kg^{-1} (80% depth-of-discharge), 500 SFUDS cycles, and US$ 150 per kWh. At present, the major drawback of the lead/acid system is its relatively low energy density; this limits severely the driving range of EVs when powered by such batteries. One approach towards overcoming this problem is to devise appropriate methods for the rapid charging of lead/acid batteries during EV duties. For practical purposes, this involves reducing charging times from

* Corresponding author.

SSDI 0378-7753(94)01988-8

the hitherto usual period of hours to the order of minutes. Considerable research effort is being directed towards the development of procedures ('algorithms') and equipment that will achieve this goal without imparting any adverse effects on battery cycle life. In work reported recently [1], the Norvik Minit-Charger™ (a device based on a constant, resistance-free voltage, charging technique [2]) has been employed to examine the rapid-charging ability, and concomitant temperature effects, of both flooded and valve-regulated lead/acid batteries [3–5].

In a previous study, we reported [6] the application of pulsed-current techniques to the formation of lead/acid battery plates. The results showed that the efficiency of the process was 15–30% greater with a pulsed-current than with an invariant-current schedule. Moreover, the high instantaneous current required by the pulsed technique can be applied without causing any undue degradation of the plate active material. With a high pulsed current, the oxidation will proceed faster and, thus, the formation time will be shortened. It is necessary, however, for the positive and negative plates to have initially a certain degree of conductivity in order to carry the applied current. Unlike discharged plates, the cured positive and negative materials have a very low conductivity during the early stages of formation and, consequently, high pulsed currents cannot be used effectively. It is considered, therefore, that pulsed-current techniques may offer a more promising approach to the rapid recharging of lead/acid batteries during service operations.

The work reported here is the first stage of a research programme that aims to examine the effect(s) of pulsed-current, rapid charging on the electrochemical characteristics and cycle-life performance of lead/acid batteries of both flooded-electrolyte and valve-regulated designs. Due to current limitations with the existing in-house hardware, preliminary studies have been performed on low-capacity automotive batteries. Furthermore, since it is well known [7] that a progressive decay in battery capacity is intensified by the application of a cycling procedure that employs a high-rate discharge followed by constant-current charge at low rates, repetitive reserve-capacity cycling at the *C*/0.8 to *C*/2 rate has been adopted in order to obtain early demonstrations of the influence of pulsed-current charging.

2. Experimental

2.1. Plate preparation

Paste was made by combining Barton-pot leady oxide, sulfuric acid and water in the proportions given in Table 1. The resulting mixture had a density of 3.9–4.0 g cm^{-3}. After mixing, the paste was applied evenly by hand (using a poly(vinyl chloride) plate) to four types of positive grids that differed in alloy composition and/or dimensions (Table 2). Note, hereafter in the text, the number preceding each minor element in the alloy denotes the content, in wt.%, of that element.

Table 1
Paste formulation for positive-plate material

Leady oxide (kg)	1.5
Water (cm^3)	235
1.4 sp. gr. H_2SO_4 (cm^3)	142
Acid-to-oxide ratio (%)	6.6
Paste density (g cm^{-3})	3.9–4.0

Table 2
Formation conditions for cells made with different grid alloys

Grid type	Alloy component	Grid dimension [a] (mm)			Current (A)	Formation time (h)
		W	H	T		
G1	1.7Sb	150	100	1.8	1	48
G2	0.09Ca–0.3Sn	143	121	3.1	1.9	20
G3	1.7Sb	105	132	1.8	1.25	20
G4	0.09Ca–0.3Sn	105	132	1.8	1.25	20

[a] W = width; H = height; T = thickness.

After pasting, the plates were mounted vertically in a stainless-steel rack in which adjacent plates were allowed to touch each other in order to simulate the curing conditions that are commonly encountered in battery manufacture. The rack was placed in a petri dish that contained a small amount of distilled water and was enclosed by a large upturned beaker. For plates prepared from grid G1, curing was performed at 90 °C with 100% relative humidity (r.h.) for 10 h, followed by processing at 40 °C with ambient humidity for a further 14 h. This procedure resulted in the development of active material that was rich (~65 wt.%) in tetrabasic lead sulfate ($4PbO \cdot PbSO_4 = 4BS$). For plates produced from grids G2–G4, curing was carried out in a single stage at 50 °C with 100% r.h. for 24 h. These conditions promoted the formation of 35 to 40 wt.% tribasic lead sulfate ($3PbO \cdot PbSO_4 \cdot H_2O = 3BS$). After curing, all the plates were dried at 75 °C until the moisture content fell below 0.1 wt.%.

The plates were grouped into 2 V cells that comprised one positive (enclosed in a Daramic separator envelope) and two negatives. The negatives were manufactured under factory conditions. Sulfuric acid solution (1.250 sp. gr.) was introduced and the plates were allowed to stand in this solution for 30 min at 25 °C. The formation process was then commenced according to the schedule given in Table 2. At the end of formation, the specific gravity of the acid had increased to about 1.270.

After formation, each cell was kept at open circuit for 30 min at 25 °C. A constant current was applied until the terminal voltage and acid density exhibited no appreciable change (i.e., within ±3%) between three, consecutive, hourly readings. This condition was taken as the initial fully-charged state of the cell. A charging current of 0.83 A/plate was used for cells prepared from grid G1 and 0.73 A/plate was applied for cells with grids G2, G3 or G4, as recommended by the respective manufacturers of commercial batteries with these grid types. The acid density was adjusted to lie between 1.265 and 1.275 g cm^{-3}.

2.2. Repetitive reserve capacity

Cells made from grids G1 or G2 were placed in a water bath that was maintained at 25 °C. By contrast, cells prepared from grids G3 or G4 were kept at either ambient conditions (i.e., ~20 °C, in order to determine the full extent of any temperature changes during charge/discharge) or 30 °C (to examine the effect of temperature on cycle life). The cell was discharged at the reserve-capacity rate (i.e., equivalent to 25 A for a 12 V battery) until the terminal voltage fell to 1.75 V. The test was repeated with invariant- or pulsed-current charging (charge-to-discharge ratio: 1.2) until the measured cell capacity was equal to 50% of the rated value given by the respective grid (battery) manufacturers, viz., 0.084 Ah g^{-1}. It should be noted, however, that under the standard specifications of the reserve-capacity test, a fixed rate of 25 A per 12 V battery is set, irrespective of the size and the number of the plates in the component cells. For the above experimental three-plate cells, the discharge current was 4.2 A for those with grid G1 and 6.25 A for those with grids G2, G3 or G4.

For pulsed-current recharge, a programmable function generator (Wavetek, model 175) was used in conjunction with battery-cycling equipment that was designed and constructed in the CSIRO laboratories. The whole system was controlled by an IBM-compatible computer (486 DX) that utilized a 'work bench' software package. Both the charging current and the voltage were also monitored on an oscilloscope (Philips, model PM3335) and the resulting waveforms were recorded on an Epson FX-870 printer. A 25% duty cycle (=on-time/(on-time+off-time)×100) was used in all the pulsed-current experiments.

2.3. Characterization of materials

The X-ray peak intensities of the constituents of the positive-plate material were measured on a standard Philips PW1710 diffractometer. The instrument was fitted with a curved graphite monochromator and used Cu Kα radiation. The phase compositions were determined by PEAKS® – an advanced, quantitative, X-ray diffraction method that has been developed in the CSIRO laboratories [8]. The morphology and the cross-sectional structure of the plates were both examined with a JEOL JSM-25S III scanning electron microscope (SEM) [6]. Electron probe microanalysis (EPMA) of plate materials was conducted on a Cameca Camebax 'microbeam' instrument that was operated at an accelerating voltage of 15 kV and a beam current of 60 nA. Data were acquired and processed under software control by means of the PC-MICROBEAM™ version 1.0 that has been developed in the CSIRO laboratories [9].

3. Results and discussion

3.1. Effect of pulsed-current charging on cycle life

The cycle-life performance of cells prepared from 4BS-cured plates using Pb–1.7Sb grids (grid G1) is shown in Fig. 1. As stated above, after each discharge, the cells were returned to 120% of charge with either an invariant- or a pulsed-current procedure. For an invariant-current charge of 0.83 A/plate (curve a), the reserve capacity of the cell at first increased steadily but then declined sharply after ~10 cycles. At this stage, the time taken to bring the cell to a fully-charged state was ~12 h. After ~17 cycles, the cell exhibited 50% of its rated reserve capacity.

In order to reduce the charging time from 12 to 1.2 h, the charging current was increased to 8.3 A/plate, i.e., 10 times higher than the normal rate for this cell. The results show that the cell suffered a severe degradation in capacity and survived for only 5 cycles (curve b). The failure of the cell was due to extensive shedding of positive active material, presumably invoked by the severe gassing that would have been experienced at the applied high rate of charging.

For pulsed-current charging at the same average current of 8.3 A/plate (on-time 1 ms, off-time 3 ms),

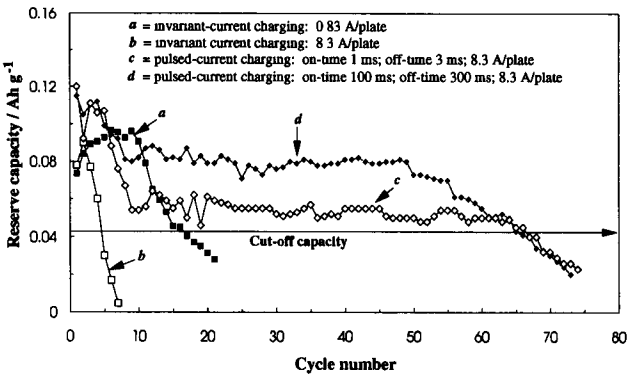

Fig. 1. Effect of pulsed-current charging on cycle life of cells prepared from 4BS-cured plates with Pb–1.7Sb grids (grid G1). Test temperature = 25 °C.

the cell capacity reported a high initial capacity, but this rapidly decreased to a low level during the subsequent 10 cycles (curve c). The cell capacity then remained virtually constant for a long period of cycling before reaching the 50% cut-off value at 65 cycles. An improved capacity performance was observed (curve d) when the on-time was increased to 100 ms and the other parameters (i.e., duty cycle, average current) were kept the same. The resulting cycle life (namely, 66 cycles) was very close to that obtained with an on-time of 1 ms. These observations indicate that the pulsed-current technique not only reduces charging time (from 12 to 1.2 h) but also exerts a significant beneficial impact on the endurance of lead/acid batteries under the duty schedule that has been applied here.

Fig. 2 shows the cycle life of cells prepared from 3BS-cured plates using Pb–0.09Ca–0.3Sn grids (grid G2). For invariant-current charging at 0.73 A/plate (curve a), the initial capacity of the cell was constant for 17 cycles. The performance then declined rapidly and the cell failed within a further 5 cycles. For pulsed-current charging at an average current of 7.3 A/plate (i.e., 10 times greater than the invariant current), the application of a short on-time (10 ms, curve b), caused a premature loss in capacity such that the life of the cell was only 8 cycles. An autopsy revealed, however, that the positive and negative plates of the cell were both still in a good mechanical condition. By contrast, the cells displayed a high and virtually constant capacity (up to 50 cycles) when a longer on-time, i.e., 100 or 200 ms, was used (curves c and d). In addition, both cells enjoyed a long (and similar) cycle life, namely, 77 and 79 cycles for an on-time of 100 and 200 ms, respectively.

It should be pointed out, however, that it is not appropriate to compare directly the cycle life obtained from the above two types of grid (viz., Pb–Sb and Pb–Ca–Sn) because of the differences in both the dimensions and the curing procedures. Therefore, the next stage was to evaluate the cycleability of cells constructed from plates that had either Pb–Sb or Pb–Ca–Sn grids with the same dimensions, and that had been prepared under the same curing conditions.

The capacity and cycle-life performances of cells prepared from 3BS-cured plates using Pb–1.7Sb grids (grid G3) are shown in Fig. 3. It can be seen that the capacity of the cell decreased steadily when an invariant-current charging regime (0.73 A/plate) was employed (curve a). The decline in capacity was 0.0025 Ah g^{-1} per cycle and the cell failed after 24 cycles. By contrast, the average value of the capacity was virtually constant over 27 cycles when applying pulsed-current charging with an equivalent invariant-current component of 7.3 A/plate but with different on-times (curves b, c and d). The endurance of the cells was: 52 cycles for an on-time of 10 ms; 64 cycles for an on-time of 100 or 200 ms. These results are similar to those reported above for cells with Pb–1.7Sb grids and 4BS curing (cf., Figs. 1 and 3).

The performance of cells prepared from 3BS-cured plates using Pb–0.09Ca–0.3Sn grids (grid G4) is presented in Fig. 4. The decline of capacity was 0.0084 Ah g^{-1} per cycle and the cell survived for only 8 cycles when charging under the invariant-current procedure (curve a). Compared with equivalent cells made from

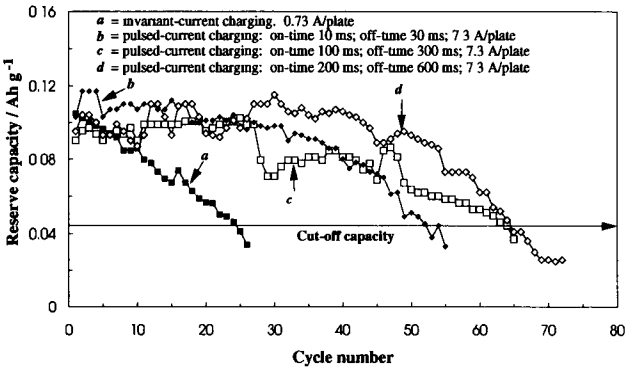

Fig. 3. Effect of pulsed-current charging on cycle life of cells prepared from 3BS-cured plates with Pb–1.7Sb grids (grid G3). Test temperature = 20 °C.

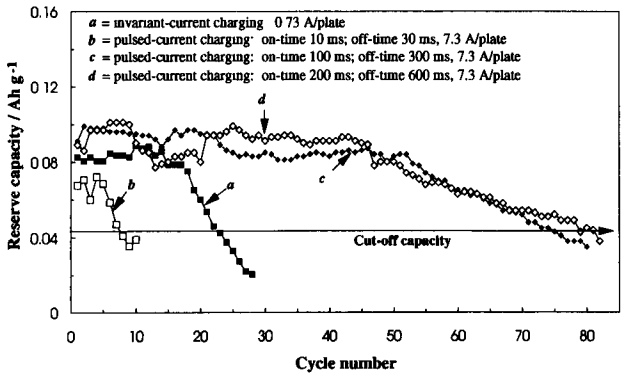

Fig. 2. Effect of pulsed-current charging on cycle life of cells prepared from 3BS-cured plates with Pb–0.09Ca–0.3Sn grids (grid G2). Test temperature = 25 °C.

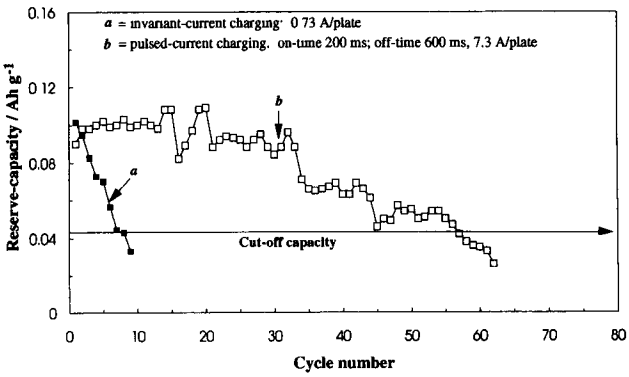

Fig. 4. Effect of pulsed-current charging on cycle life of cells prepared from 3BS-cured plates with Pb–0.09Ca–0.3Sn grids (grid G4). Test temperature = 20 °C.

Pb–Sb grids (grid G3, Fig. 3), the decrease in capacity was more rapid and the cycle life was much shorter, cf., 0.0084 with 0.0025 Ah g^{-1} per cycle, and 8 with 24 cycles. Cells based on Pb–Ca–Sn grids delivered a nearly constant capacity over the first 30 cycles and lasted for 57 cycles when pulsed-current charging with an on-time of 200 ms was employed. This cycle-life performance is similar (but the overall capacity is lower) to that delivered by Pb–Sb cells (Fig. 3) and, hence, leads to the important conclusion that pulsed charging is an effective means of suppressing the phenomenon of premature capacity loss that is more commonly experienced with Pb–Ca cells [10].

Finally, it is of practical importance to examine whether the pulsed-current charging technique can recover the capacity that is lost during cycling under invariant-current charging. Fig. 5 gives an example of the influence of intermittent periods of pulsed-current charging on the capacity of cells (grid G3, 3BS curing) that were first subjected to invariant-current charging at 0.73 A/plate. Under invariant current, the capacity of the cell decreased steadily with cycling and reached 80% of the initial value after 6 cycles. The initial level of capacity, however, was virtually recovered within a further 5 cycles when a pulsed-current regime (on-time 100 ms; average current 7.3 A/plate) was applied. The capacity decreased again on switching back to the original invariant-current recharge. The capacity was allowed to fall to 60% before returning to the pulsed-current recharge. Although no improvement in cell performance was observed, the previous sharp decline in capacity was arrested and the value remained at the 60% level. The capacity continued to decrease to the cut-off value when invariant-current charging was re-introduced.

In summary, it can be concluded that the pulsed-current technique can exert highly advantageous effects – not only on the rate of recharge but also on the cycle-life performance of lead/acid batteries, especially when an on-time of greater than 100 ms is used. Furthermore, this technique can also rejuvenate cells that have been cycled with invariant-current charging.

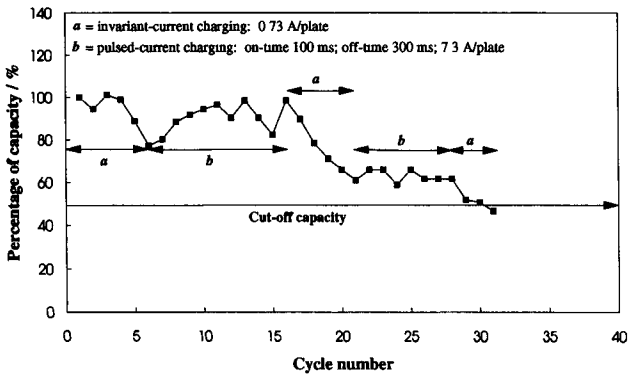

Fig. 5. Recovering capacity: periodic application of pulsed-current charging to cycled cell with 3BS-cured plates and Pb–1.7Sb grids (grid G3). Test temperature = 20 °C.

3.2. Charging characteristics of invariant- and pulsed-current techniques

Fig. 6 shows the applied current and resulting voltage waveforms during the initial and final stages of the pulsed-current charging of cells with Pb–0.09Ca–0.3Sn grids (grid G2) and 3BS-cured plates. There is a sudden increase in voltage (i.e., an *IR* effect) immediately the pulsed current is switched on (Fig. 6(a), (b)). The voltage continues to rise slowly during the on-time. Similarly, there is a sharp fall in voltage when the current is removed; the cell resistance can be determined from the associated *IR* drop. Thereafter, the cell voltage decreases more slowly. A comparison of the voltage waveform at the beginning and the final stages of pulsed-current charging provides the following general observations.

- At the final stages of charging, the amplitude of the *IR* effect becomes smaller. As expected, this indicates that the cell resistance decreases with charging time due to the conversion of $PbSO_4$ to PbO_2. In the above experiments, the resistance was 12–15 mΩ at the beginning of charging, and 4–7 mΩ at the end. Similar ranges of values were also obtained for cells with Pb–Sb grids.

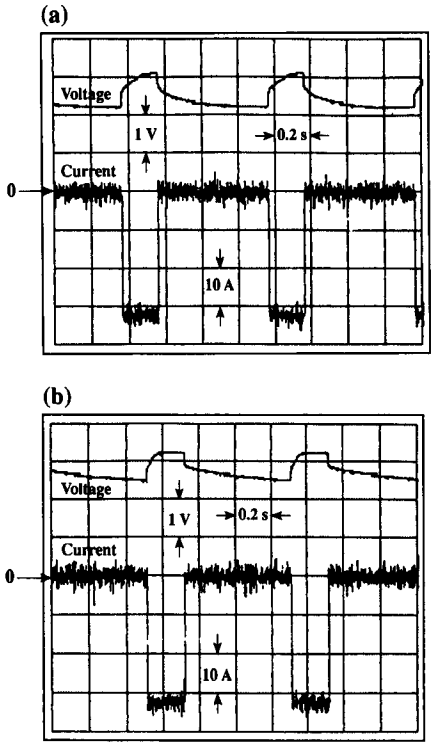

Fig. 6. Applied current and resulting voltage at (a) initial and (b) final stages of pulsed-current charging for cells with Pb–0.09Ca–0.3Sn grids (grid G2) and 3BS curing. Test temperature = 25 °C.

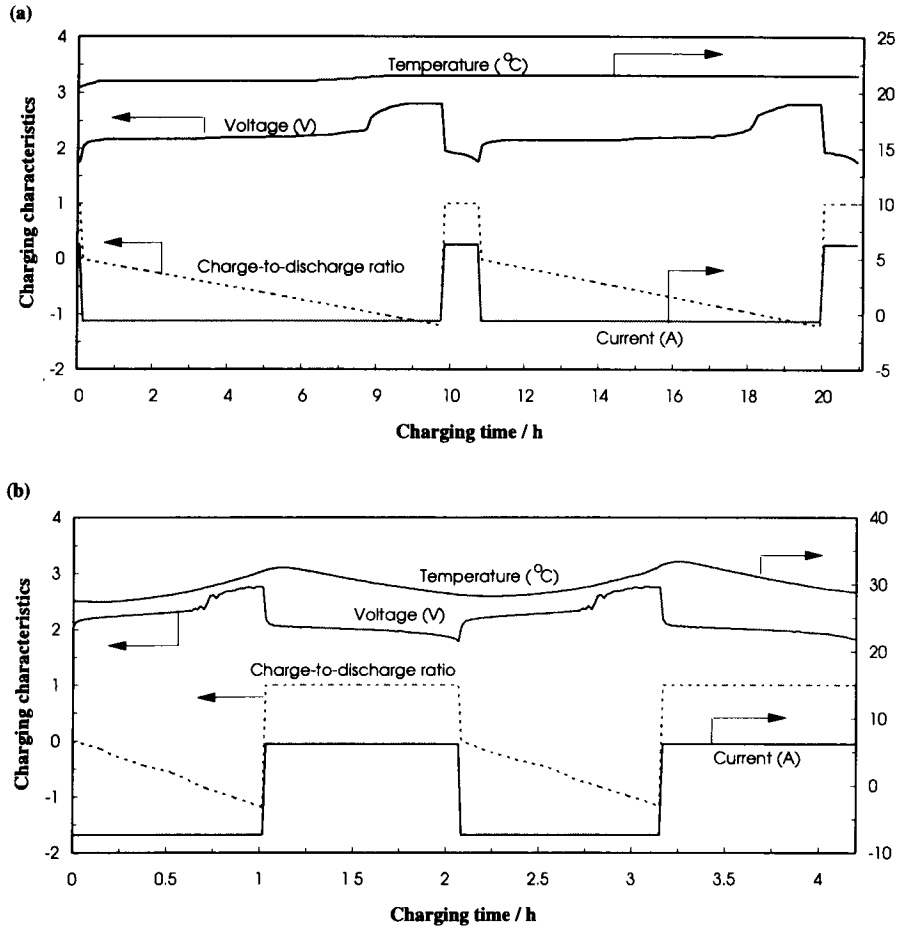

Fig. 7. Change in current, voltage and electrolyte temperature of cells with Pb–0.09Ca–0.3Sn grids (grid G4) and 3BS curing: (a) invariant-current charging; (b) pulsed-current charging. Note, with format used here, negative ordinate values refer to charging current, positive values to discharging current. Thus, the charge-to-discharge ratio is shown to increase in a negative sense.

• At the final stages of charging, the voltage during the on-time rises more rapidly and becomes flatter, while the voltage at the end of the off-time is higher. This reveals that the overall level of the voltage waveform is increased as the charging proceeds.

The change in current, voltage and electrolyte temperature of a cell with Pb–0.09Ca–0.3Sn grids (grid G4) during invariant- (i.e., 0.73 A/plate) and pulsed-current charging (on-time 200 ms, off-time 600 ms, average current 7.3 A/plate) is presented in Fig. 7. Note, the current and voltage curves in Fig. 7(b) are the average values of the corresponding pulsed current and voltage at the time of sampling (i.e., 2 min intervals). Results show that: (i) the change in the average voltage during pulsed-current charging follows a similar trend to that observed during invariant-current charging; (ii) the charging time is reduced significantly, from ~10 to ~1 h, when using pulsed-current charging; (iii) there is a noticeable increase in the electrolyte temperature with pulsed-current charging.

It has been established [11] that the capacity and cycle-life performance of batteries can be enhanced by an increase in electrolyte temperature up to ~50 °C. Therefore, it must be determined whether the cycle-life improvement with pulsed-current charging is not simply a temperature effect. Consequently, the following experiments were performed to evaluate the repetitive reserve capacity of cells subjected to invariant-current charging at an elevated temperature, i.e., at a value around that reached by cells when pulsed charged (namely, ~30 °C, Fig. 7) under the above ambient conditions (i.e., ~20 °C).

3.3. Effect of temperature on cycle life

A comparison of the cycle-life performance of cells (3BS curing) with invariant-current recharge at 20 and 30 °C is presented in Fig. 8. For cells prepared from Pb–1.7Sb grids, the level of capacity was higher and the rate of decline in capacity with cycling was smaller (viz., 0.0015 versus 0.0025 Ah g^{-1} per cycle) when cycling was performed at 30 °C. Consequently, longer life was obtained from cells operated at 30 °C (i.e., 43 versus 24 cycles). For cells made from Pb–0.09Ca–0.3Sn grids, the capacity at 30 °C was higher than that at 20 °C, but the initial rapid decline during the first 6 cycles at each temperature was very similar. After that, the degradation in capacity at 30 °C slowed down and,

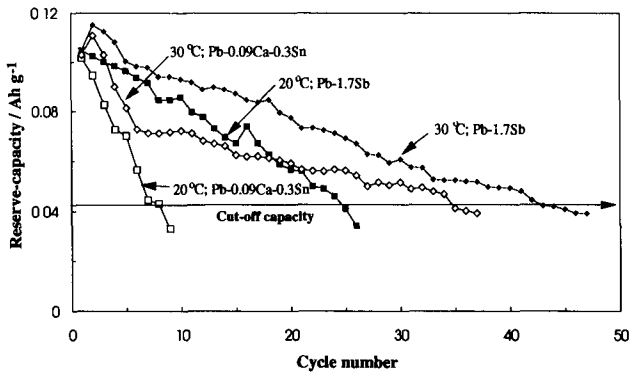

Fig. 8. Effect of temperature on cycle life of cells (3BS curing) with invariant-current charging.

therefore, the cells exhibited longer life than those cycled at 20 °C (i.e., ~35 versus 8 cycles).

These results confirm that an increase in the electrolyte temperature can indeed enhance the cycle life of cells. Nevertheless, the improved performance at 30 °C falls well short of that obtained with pulsed-current charging (namely: 64 cycles for Pb–1.7Sb, Fig. 3; 57 cycles for Pb–0.09Ca–0.3Sn, Fig. 4). This suggests that the extension of battery life given by the pulsed-charging technique is due not only to a concomitant increase in temperature, but also to other more important factors that have yet to be identified.

The negative plates appeared to be in a good condition after failure. By contrast, the positive plates displayed both different degrees of material softening and various amounts of material shedding. Loss of material occurred at both the upper regions and the periphery of the plates. The extent of material instability was dependent upon the type of grid alloy (i.e., Pb–Sb or Pb–Ca–Sn), the charging regime (i.e., invariant or pulsed current), the electrolyte temperature, and the number of cycles that a given cell had performed.

With Pb–Sb grids, only a small quantity of material was dislodged from the upper regions of the plates when cycling was performed under invariant charging at either room temperature or 25 °C. The degradation was extended to the outer edges at the higher temperature of 30 °C and was more severe (i.e., ~50% loss) than that observed with pulsed-current charging at either room temperature or 25 °C (i.e., ~10–15% loss, together with overall softening of material).

With Pb–Ca–Sn grids, the positive plates exhibited no major displacement of material when the cells were cycled under invariant current at either room temperature (i.e., ~20 °C) or 25 °C. By contrast, about 10% of the material was shed from the edges of the plates in cells that had failed under invariant-current charging at 30 °C or under pulsed-current charging at room temperature or 25 °C.

Based on the above observations of material shedding and softening in positive plates, it can be concluded that premature capacity loss occurs when cells are cycled at high rates of discharge with invariant-current charging at either room temperature or 25 °C, irrespective of the type of grid alloy. This decline in performance appears earlier for cells that use Pb–Ca–Sn grids, as opposed to Pb–Sb counterparts (see Fig. 8).

3.4. Structure of positive active material and corrosion layer

In the following studies, examinations were made of both the morphology of the active material and the nature of the grid corrosion layer in positive plates that were sampled in the charged state. It should be noted, however, that plates after initial charging retain about 10–12 wt.% $PbSO_4$. This level decreases to 4–6 wt.% and remains unchanged after a few cycles (i.e., 5 cycles), regardless of the applied charging regime and the type of grid alloy. In contrast to plates that have failed after duty at room temperature or 25 °C, plates at 30 °C contain no residual $PbSO_4$ (see Table 3).

3.4.1. Pb–0.09Ca–0.3Sn grids

The morphology of the positive active material in positive plates with Pb–0.09Ca–0.3Sn grids (grid G4) and after recharging with invariant current or pulsed current is shown in Figs. 9 and 10, respectively. Following initial charging, the active material is composed of irregular-shaped ('cauliflower') agglomerates with small, needle-like crystals protruding from the surface (Fig. 9(a)). At higher magnification, micrographs reveal that the crystallinity of the material is not well-defined (Fig. 9(b)). At an operating temperature of 20 °C, the macroscopic structure persists during the first 5 cycles, but there is evidence of greater numbers of individual, longer crystals on the surface (Fig. 9(c)). At subsequent cell failure, these acicular crystals are found to have been replaced by elongated, equi-axial counterparts (Fig. 9(d)). Overall, the structure of failed plates displays a higher degree of crystallinity compared with that in fresh plates (cf., Fig. 9(d) with (a), (b)). The crystallinity becomes more prominent, i.e., the crystals grow to larger sizes, when plates are cycled to failure at 30 °C (Fig. 9(e), (f)). In addition, the surface roughness of the PbO_2 crystals is found to decrease with the increase in crystal size (Fig. 9(f)). Similar changes in crystal

Table 3
Phase composition (wt.%) of positive plates in a charged state

	β-PbO_2	$PbSO_4$
Plates in initial fully-charged state	88–90	10–12
Plates after 5 cycles and up to cell failure, at room temperature or 25 °C	94–96	4–6
Plates in failed cells at 30 °C	100	

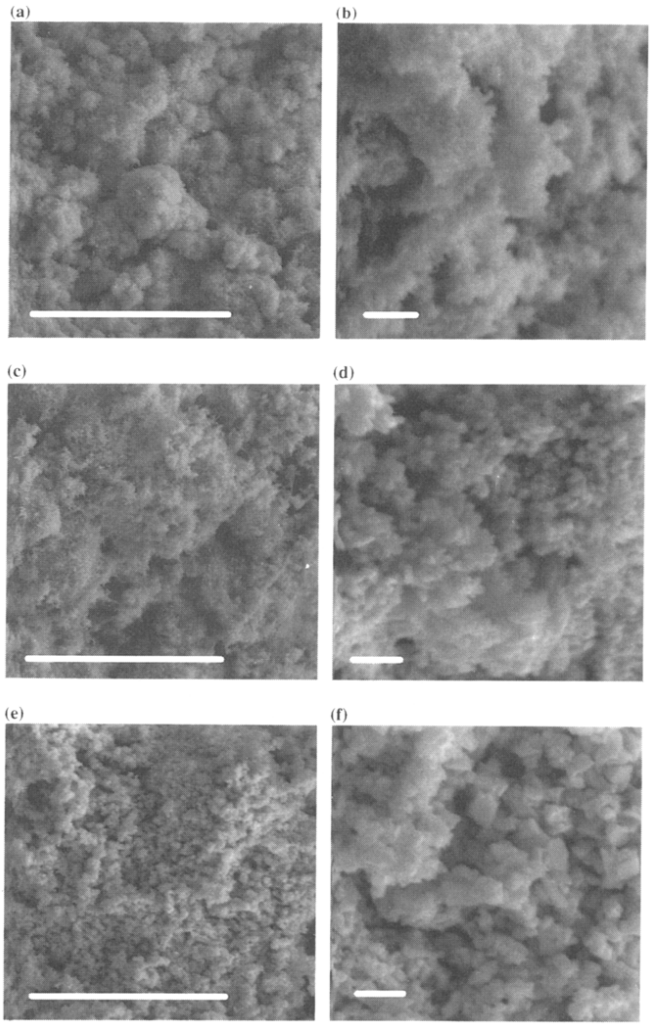

Fig. 9. Electron micrographs of active material in positive plates with Pb–0.09Ca–0.3Sn grids (grid G4) and recharged by invariant current: (a), (b) after initial charging at 25 °C; (c) after 5 cycles at 20 °C; (d) after failure at 20 °C; (e), (f) after failure at 30 °C. Magnification bar: (a), (c), (e) 10 μm; (b), (d), (f) 1 μm.

structure have been reported [12] for cycled, positive plates in valve-regulated lead/acid batteries.

With pulsed-current charging (on-time 200 ms, off-time 600 ms, average current 7.3 A/plate), the broad features of the initial agglomerate structure of the positive plate are retained for longer periods (24 cycles, cf., Fig. 10(a) and (b)). When the cell reaches the failure point, the structure of the active material exhibits greater crystallinity and equi-axial, elongated PbO_2 crystals are developed (Fig. 10(c), (d)). This change in morphology is similar (but the crystals are smaller in size) to that observed above in failed cells that have been subjected to invariant-current charging, even though the pulsed-current cells have endured a much longer cycle life (c.f., Fig. 10(c), (d) with Fig. 9(d), (e), (f)).

Cross-sectional views of cycled plates with Pb–0.09Ca–0.3Sn grids (grids G2 and G4) and recharged with invariant current are presented in Fig. 11. Im-

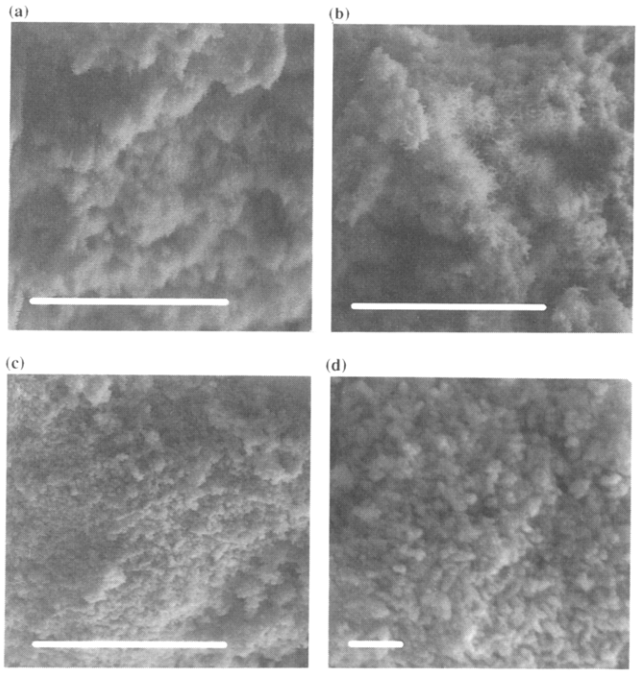

Fig. 10. Electron micrographs of active material in positive plates with Pb–0.09Ca–0.3Sn grids (grid G4) and recharged by pulsed current, i.e., on-time 200 ms, off-time 600 ms, average current 7.3 A/plate: (a) after initial charging at 25 °C; (b) after 24 cycles at 20 °C; (c), (d) after failure at 20 °C. Magnification bar: (a), (b), (c) 10 μm; (d) 1 μm.

mediate inspection shows (Fig. 11(a)) that the corrosion layer is comprised of two distinct regions: (i) a dense, continuous, inner layer immediately adjacent to the grid; (ii) a porous, outer layer. The inner layer is found to have a composition in the range $PbO_{1.0}$ to $PbO_{1.2}$, denoted hereafter as 'PbO'. By contrast, the porous, outer layer is composed mainly of lead dioxide (i.e., $PbO_{1.8}$ to $PbO_{2.0}$). At higher magnification, micrographs reveal that a third and dense layer resides between the inner and outer layers (Fig. 11(b)). This layer appears to be attached more firmly to the inner corrosion product than to the outer material. Data from EPMA analysis indicate that this layer has a composition of $n(PbO_2)\cdot PbSO_4$ with $n = 1$–2.

Similar phenomena are observed in failed plates with Pb–Ca–Sn grids (grids G2 and G4) that have been cycled under pulsed-current charging (on-time 200 ms, off-time 600 ms, average current 7.3 A), see Fig. 12(a). The continuous, inner 'PbO' corrosion layer is, however, slightly thinner than that formed under invariant-current conditions. In addition, close inspection shows (Fig. 12(b)) that the inner corrosion layer is discontinuous and is separated into a series of 'islands'.

3.4.2. Pb–1.7Sb grids

The morphology of active material in positive plates using Pb–1.7Sb grids (grid G3) and recharged under invariant-current or pulsed-current conditions is pre-

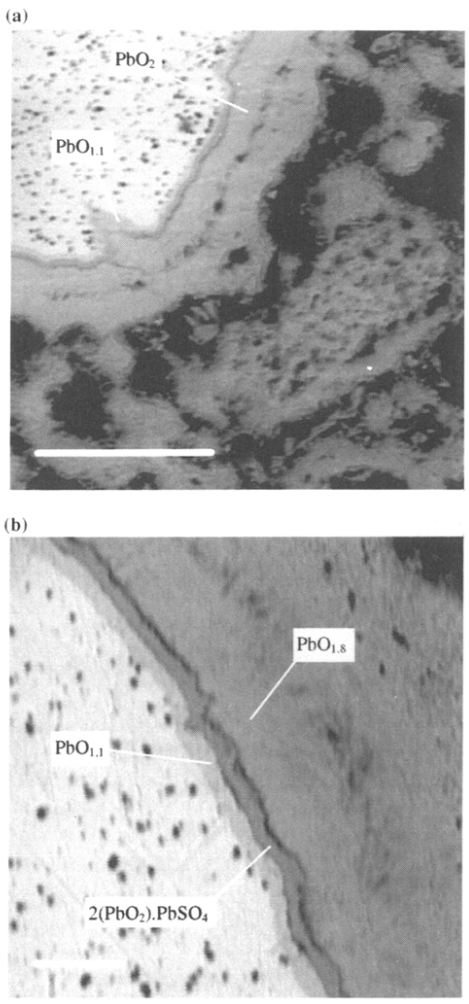

Fig. 11. Cross-sectional views of cycled plates with Pb–0.09Ca–0.3Sn grids and recharged by invariant current: (a) grid G4; (b) grid G2. Magnification bar: (a) 50 μm; (b) 10 μm.

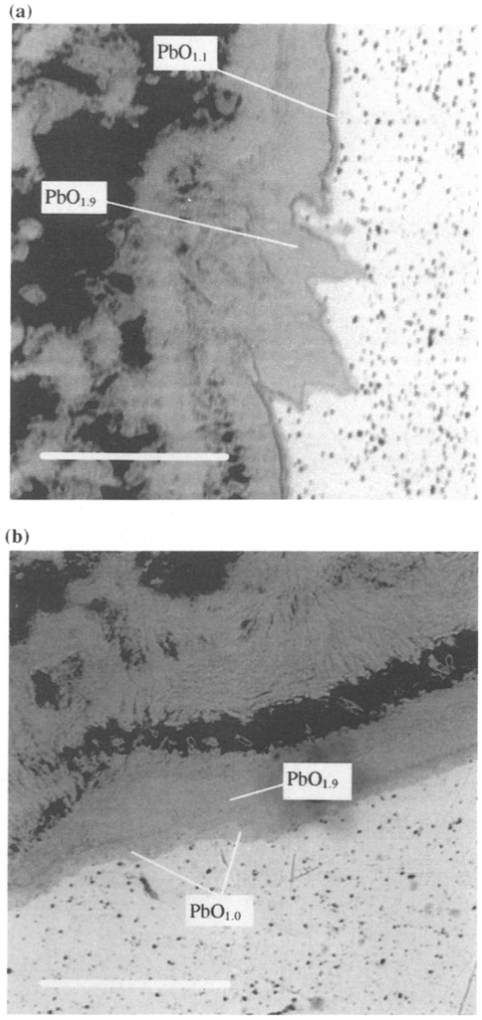

Fig. 12. Cross-sectional views of cycled plates with Pb–0.09Ca–0.3Sn grids and recharged by pulsed current, i.e., on-time 200 ms, off-time 600 ms, average current 7.3 A/plate: (a) grid G4; (b) grid G2. Magnification bar: 50 μm.

sented in Figs. 13 and 14, respectively. The microstructure of positive plates after initial charging is similar to that of plates prepared from Pb–0.09Ca–0.3Sn grids, namely, cauliflower agglomerates with fine, needle-like crystals on the surface (Fig. 13(a)). With invariant-current charging, these acicular crystals become shorter and are reduced in number as cycling proceeds (Fig. 13(b), (c)). Eventually, equi-axial, elongated crystals are developed in plates at failure (Fig. 13(d)). Failed plates cycled at 30 °C display more crystallinity than those operated at 20 °C (cf., Fig. 13(e) with (f)). Moreover, the crystal size in failed plates at 30 °C is smaller than that in failed plates with Pb–0.09Ca–0.3Sn grids at the same operating temperature (cf., Fig. 13(f) with Fig. 9(f)).

Under the action of pulsed-current charging (i.e., on-time 200 ms, off-time 600 ms, average current 7.3 A/plate), the microstructure of the active material again undergoes a marked change from fine, acicular crystals in initially charged plates (Fig. 14(a)) to equi-axial, elongated crystals in failed plates (Fig. 14(c)). Note, due to experimental limitations, the exact cycle number at which the prismatic crystals start to develop is unknown. It is clear, however, that the acicular crystals are maintained up to 24 cycles (Fig. 14(b)). At failure, the crystal size in Pb–Sb plates is generally smaller under the action of pulsed charging, cf., Fig. 14(c) with Fig. 13(d).

Cross-sectional views of cycled plates with Pb–1.7Sb grids (grid G1) and recharged under invariant or pulsed current are presented in Fig. 15. It can be seen that there is little difference in the corrosion layer that is formed under the two types of charging (cf., Fig. 15(a) with (b)). In both cases, the layer is composed of zones with different phases compositions. Furthermore, a continuous void is found to exist close to the grid surface.

3.5. Change in BET surface area of active material with cycling

The BET surface areas of both initially charged and cycled positive active materials from cells with different

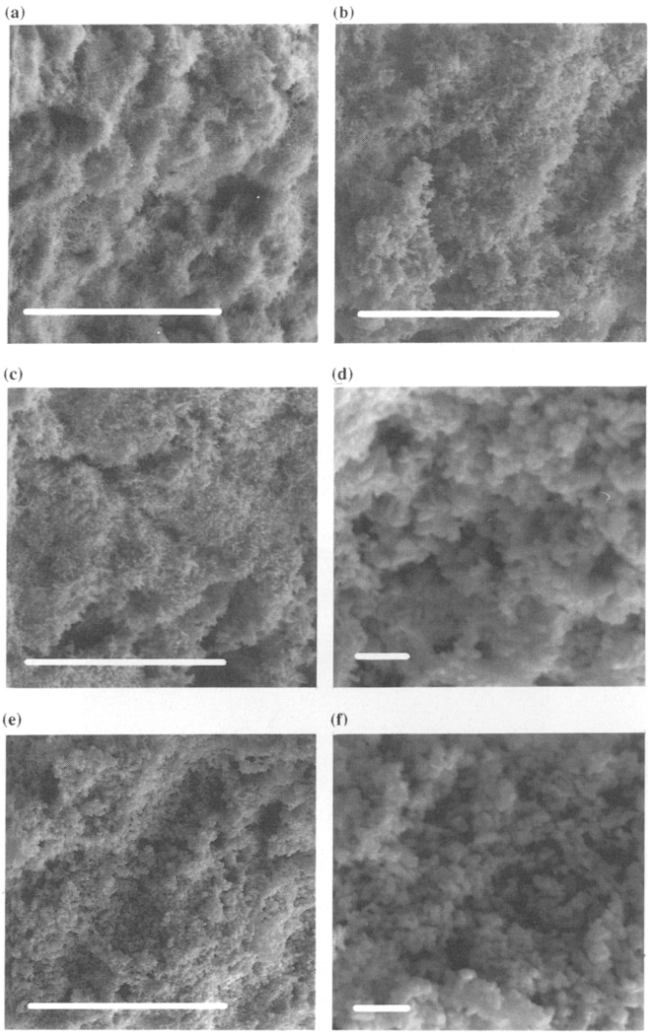

Fig. 13. Electron micrographs of active material in positive plates with Pb–1.7Sb grids (grid G3) and recharged by invariant current: (a) after initial charging at 25 °C; (b) after 5 cycles at 20 °C; (c) after 16 cycles at 20 °C; (d) after failure at 20 °C; (e), (f) after failure at 30 °C. Magnification bar: (a), (b), (c), (e) 10 μm; (d), (f) 1 μm.

grid alloys, charging regimes and electrolyte temperatures are presented in Fig. 16. The data show that the surface area of fresh materials prepared from Pb–Ca–Sn grids is lower than that prepared from Pb–Sb varieties, namely, 7.39 versus 8.29 $m^2\ g^{-1}$. For both Pb–Ca–Sn and Pb–Sb cells cycled at 20 °C under invariant-current charging, the BET surface area decreases with cycling but the effect is less marked in Pb–Ca–Sn cells. At cell failure, the surface area has only decreased from 7.39 to 6.35 $m^2\ g^{-1}$ in Pb–Ca–Sn cells but has reduced significantly from 8.39 to 4.19 $m^2\ g^{-1}$ in Pb–Sb cells. This indicates that the cycled positive active material in Pb–Ca–Sn cells is in a healthier condition. There is a greater reduction in BET surface area when the cells are cycled to failure at higher temperature (i.e., 30 °C). The surface area falls to 4.35 and 3.65 $m^2\ g^{-1}$ in Pb–Ca–Sn and Pb–Sb cells, respectively. This shows that the degradation in active

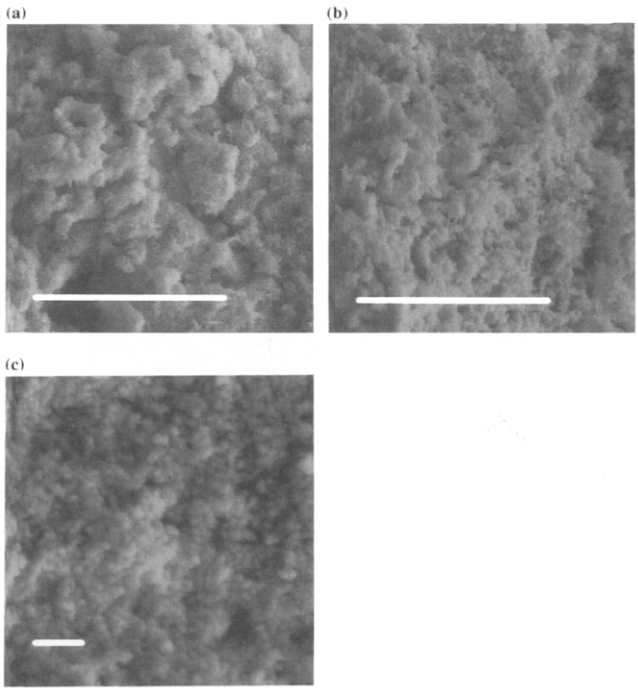

Fig. 14. Electron micrographs of active material in positive plates with Pb–1.7Sb grids (grid G3) and recharged with pulsed current, i.e., on-time 200 ms, off-time 600 ms, average current 7.3 A/plate: (a) after initial charging at 25 °C; (b) after 24 cycles at 20 °C; (c) after failure at 20 °C. Magnification bar: (a), (b) 10 μm; (c) 1 μm.

material is more severe in both cells when the charge/discharge process is prolonged. With pulsed-current charging (i.e., on-time 200 ms, off-time 600 ms, average current 7.3 A/plate) at 20 °C, the BET surface area of the failed material in Pb–Ca–Sn and Pb–Sb cells is 5.95 and 5.40 $m^2\ g^{-1}$, respectively. The lower surface area of the material in Pb–Ca–Sn cells, compared with that in cells at failure under invariant-current charging (viz., 5.95 versus 6.35 $m^2\ g^{-1}$), is almost certainly due to the fact that the former cells gave greater service (viz., 57 versus 8 cycles). It is important to note, however, that despite longer cycle life (viz., 64 versus 24 cycles), the surface area in failed Pb–Sb cells was still higher under pulsed-current charging conditions (viz., 5.40 versus 4.19 $m^2\ g^{-1}$).

In summary, the above studies show clearly that: (i) the crystallinity of the positive plates increases and the crystal habit changes with cycling, irrespective of the chosen grid alloy, charging regime or electrolyte temperature; (ii) the crystallization process during cycling is prolonged and the size of the eventual equi-axial, elongated crystals is depressed by the addition of antimony to the grid; this behaviour is intensified under the influence of pulsed-current charging; (iii) the crystals become well-defined, with smooth surfaces and larger sizes, when plates using Pb–0.09Ca–0.3Sn grids are cycled to failure at 30 °C; (iv) compared with Pb–Sb cells, the corrosion layer developed around Pb–Ca–Sn grids is more dense and contains a thin, inner corrosion

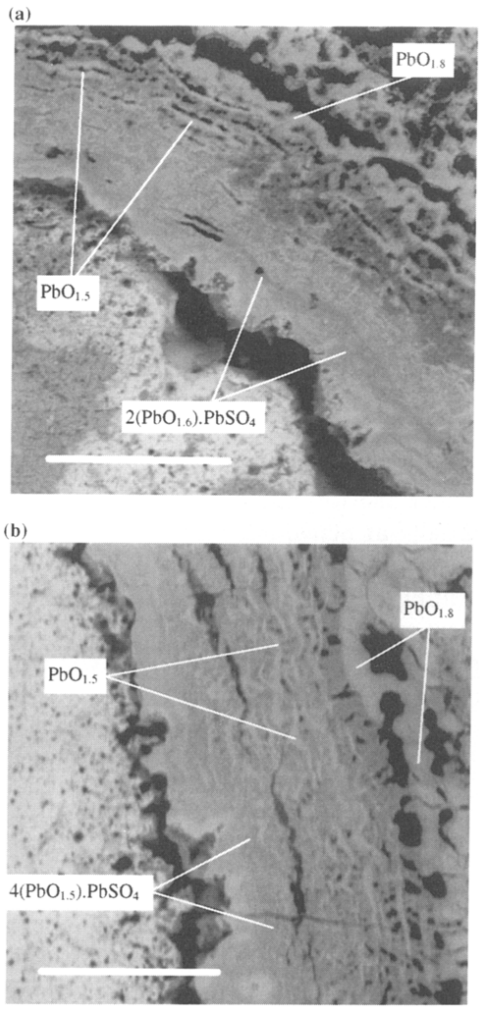

Fig. 15. Cross-sectional views of cycled plates with Pb–1.7Sb grids (grid G1): (a) invariant-current charging 0.83 A/plate; (b) pulsed-current charging, on-time 100 ms, off-time 300 ms, average current 8.3 A/plate. Magnification bar: 50 μm.

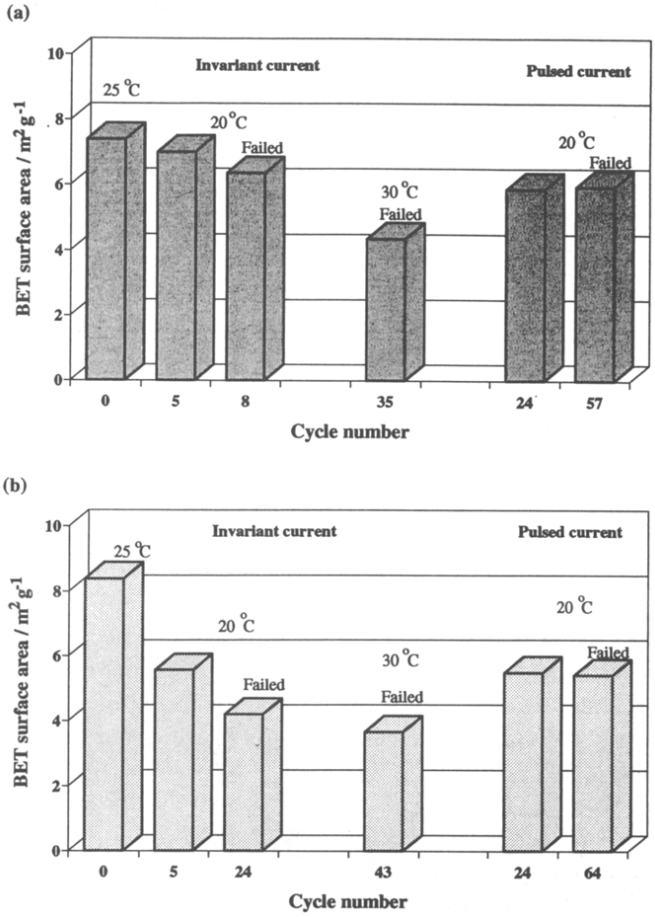

Fig. 16. Change in specific surface area of plates prepared from (a) Pb–Ca–Sn grids (grid G4) and (b) Pb–Sb grids (grid G3) with cycling at different electrolyte temperatures, and invariant-current charging (0.73 A/plate) or pulsed-current charging (on-time 200 ms, off-time 600 ms, average current 7.3 A/plate).

layer that is comprised mainly of 'PbO'; (v) the inner corrosion layer is reduced in thickness, or is divided into islands, when Pb–Ca–Sn cells are subjected to pulsed-current charging.

3.6. Effect(s) of antimony and pulsed-current charging on active material

It is evident from the above studies that premature capacity loss has taken place in both Pb–Ca–Sn and Pb–Sb cells that have been cycled at high discharge rates under invariant-current charging at 20 and 25 °C. A similar observation has been made by Hollenkamp et al. [10]. The capacity decline occurs more rapidly in Pb–Ca–Sn cells and, consequently, the cycle life is shorter than that given by Pb–Sb cells. At the point of failure, the active material is composed of equi-axial, elongated crystals and is more crystalline than that present in the precursor plates. This observation is true for all cells, irrespective of the preparation and recharging conditions. The growth of these crystals reduces the effective surface area. Moreover, Yamashita and Matsumaru [12] have demonstrated that the reactivity of the active material with sulfuric acid is decreased when such crystals are formed.

For the Pb–Ca–Sn cells, the equi-axial crystals can grow to relatively large sizes with cycling (see, Fig. 9(f)). By contrast, with either Pb–Sb cells recharged by invariant current or Pb–Ca–Sn and Pb–Sb cells recharged by pulsed current, the development of equi-axial, elongated crystals is arrested so that a relatively small size is retained at cell failure. This behaviour is more prominent in the positive active material of cells subjected to pulsed charging, even though these cells have undergone a much longer cycle life. Thus, the effect of antimony and/or pulsed charging serves to improve the capacity performance of cells.

Recently, Pavlov [13] has proposed that agglomerates of positive active material consist of α-PbO_2 and/or β-PbO_2 crystal zones, together with amorphous/hydrated $PbO(OH)_2$ gel zones. It is argued that the latter zones are composed of hydrated linear polymer chains that

provide mechanical strength, as well as both electron and proton conductivity. The gel zones have a higher resistance than the crystal zones and, thus, the overall plate conductivity depends on the concentration of the polymer chains. At the contact surface between two agglomerates, the polymer chains of the gel zone in one agglomerate merge with the polymer chains of the other to form a common chain. The current passes through the resulting 'bridge' that is formed between the two agglomerates. Accordingly, the skeleton of positive active material is a continuous system that is comprised of elements with different resistances.

Applying this theory, an increase in the crystallinity of active material during cycling is expected to result in a gradual decrease in the mechanical strength and, consequently, in a progressive decrease in the conductivity of the plates. Conversely, a slowing down of the crystallization process will prolong the service life of batteries. The studies reported here have demonstrated that the crystallization process can be arrested either by the addition of antimony to the grid alloy or, more importantly, by the application of pulsed-current charging. The latter approach exerts the stronger effect.

Swets [14] has investigated the similarity between the crystal structures of α-PbO_2 and $PbSb_2O_6$. The latter compound contains Sb^{5+} ions that are octahedrally coordinated towards the oxygen in the same manner as Pb^{4+} in α-PbO_2 and β-PbO_2. The arrangement of the octahedra in $PbSb_2O_6$ is quite similar to that in α-PbO_2. Furthermore, from an analysis of the positive active material of cycled automotive batteries, the presence of $PbSb_2O_6$ was detected in 20% of the batteries examined. Similarly, Arifuku et al. [15] concluded that the anodic layer formed on smooth lead electrodes in a Sb^{3+}-containing H_2SO_4 solution is composed of a complex oxide that contains Pb^{2+}, Sb^{5+} and O^{2-} ions, together with a relatively large amount of α-PbO_2. In these authors' opinion, however, the observed increased X-ray diffraction signals of α-PbO_2 could have been brought about by superposition of those of $PbSb_2O_6$. In other studies, Dawson et al. [16] found that Sb^{3+} ions are adsorbed much more rapidly than Sb^{5+} ions on PbO_2 and $PbSO_4$, and that the adsorption of antimony (i.e., Sb^{3+} and Sb^{5+}) on PbO_2 is substantially larger than that on $PbSO_4$. These observations clearly indicate that antimony ions, after oxidative leaching from Pb–Sb grids, become incorporated in the lattice of PbO_2 and, thereby, will modify both the size of the crystals and the macroscopic structure of the active material. Similar effect(s) of antimony on the modification of PbO_2 crystallinity and the morphology of plate active material have been observed by other authors [17–20].

It is well known that the oxidation of $PbSO_4$ to PbO_2 proceeds through a dissolution–deposition mechanism. The reaction can be described as follows:

$$PbSO_4 \rightleftharpoons Pb^{2+} + SO_4^{2-} \quad (1)$$

$$Pb^{2+} + 2H_2O \rightleftharpoons PbO_2 + 4H^+ + 2e \quad (2)$$

In general, the size of the PbO_2 crystals is determined by the respective rates of the nucleation and growth processes: the resulting crystal size will be smaller if the nucleation rate is greater than the growth rate, and vice versa. Furthermore, the nucleation rate of PbO_2 is affected strongly by several factors, namely, the concentration of the Pb^{2+} ions, the morphology of the substrate (i.e., active sites), the adsorption of foreign species (e.g., antimony, as mentioned above), and the deposition voltage.

Under normal charging conditions (i.e., no additive, low current), the formation of PbO_2 crystals will occur preferentially at active sites on the substrate because these locations require a lower energy for deposition. The resulting crystals will grow to a large size during further stages of the charging process. With high pulsed-current charging, although the average voltage is similar to that for the invariant-current procedure (see Fig. 7), the instantaneous pulsed voltage is much higher. Under this increased driving force, the nucleation of tiny PbO_2 crystals will take place both rapidly and randomly during the on-time, irrespective of defects on the substrate (e.g., steps, kinks, etc.). Furthermore, the continuous growth of these crystals will be interrupted during the current off-time. (Note, the nucleation rate is proportional to the deposition voltage, but the critical size for nucleus formation is proportional to the reciprocal of the voltage.) Thus, the PbO_2 crystals will be maintained in a less-crystalline state for a longer period of charge/discharge cycling, and the crystals will be restricted to much smaller sizes, even at the point of cell failure.

3.7. Effect(s) of antimony and pulsed-current charging on corrosion layer

Although the cycled, positive active material of Pb–Ca–Sn and Pb–Sb cells has an outwardly similar crystal structure at failure, cross-sectional examination reveals certain, distinct differences. Compared with Pb–Sb cells, the corrosion layer developed around grid members in Pb–Ca–Sn cells is more dense. A thin inner corrosion layer that is comprised mainly of an insulating 'PbO' compound is also present. This layer had been found to develop at various stages of cycle life [10]. Since the specific surface area of cycled material in Pb–Ca–Sn cells with invariant-current charging at 20 °C is much higher than that of Pb–Sb cells (a feature that should assist the capacity performance), a plausible explanation for the rapid capacity loss that is in fact observed with the former cells (cf., Figs. 3 and 4) is the development of a 'barrier' layer at the grid/active-

material interface. Indeed, Dimitrov and Pavlov [21] have recently established that the premature capacity loss of lead/acid batteries with pure-lead grids is determined by the grid/corrosion-layer interface.

An important conclusion from the studies reported here is that premature capacity loss, as well as early failure of Pb–Ca–Sn cells, can be prevented by the application of pulsed-current charging, even though a barrier layer is still present at cell failure. Under this mode of charging, however, the inner corrosion layer becomes thinner and/or is divided into islands, by comparison with the thick and continuous product formed under invariant-current charging. These results demonstrate clearly that the thickness and distribution of the barrier layer are key contributors to premature capacity loss.

The development of 'PbO' beneath a layer of $PbSO_4$ has been postulated by Pavlov and Iordanov [22] and explained by Ruetschi [23]. More recently, Culpin et al. [24] have presented a detailed, schematic mechanism for PbO formation. The $PbSO_4$ layer (or any dense layer with tiny pores) is considered to act as a semi-permeable membrane that hinders, or blocks, the movement of HSO_4^- and SO_4^{2-} ions into the corrosion layer. Deposition of sulfate species trapped beneath the semi-permeable film, together with a net flow of H^+ ions to the negative plates during charging, raise the pH in the interior of the corrosion layer and, hence, promote the reaction between Pb^+ and OH^- to form PbO (see Fig. 17). Under invariant-current charging, the net flow of H^+ ions is promoted by both migration and diffusion forces. During the off-time periods experienced under pulsed-current charging, however, this net flow of H^+ ions is affected only by the diffusion process. Therefore, the shift towards an increase in pH within the interior of the corrosion layer will be slower during pulsed-current charging. As a result, the PbO layer developed under pulsed-current charging will be thinner than that produced under invariant-current charging. Furthermore, as dictated by the roughness of the grid surface, the coverage of the thin PbO layer can be discontinuous, that is, the layer can be broken up into discrete islands. Such behaviour will serve to reduce the electrical resistance and, hence, improve the capacity performance of the cell.

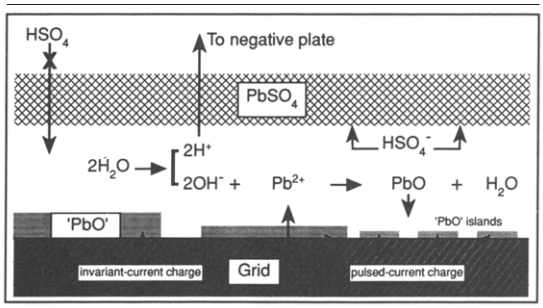

Fig. 17. Schematic diagram of the development of 'PbO' on the grid surface during cycling under invariant- or pulsed-current charging.

4. Conclusions

The objective of this initial study has been to evaluate the effect(s) of pulsed current of constant amplitude on the rapid charging and cycle-life performance of low-maintenance lead/acid batteries of an automotive design and with Pb–Sb or Pb–Ca–Sn grids. The results obtained in this work have also provided valuable information on the mechanism of premature capacity loss in both Pb–Sb and Pb–Ca–Sn cells with conventional invariant-current charging. The major findings can be summarized as follows:

- pulsed-current charging techniques can exert highly advantageous effects – not only in terms of accelerating battery recharge but also with respect to extending the cycle-life performance of low-maintenance batteries;
- recharging time can be reduced by an order or magnitude, i.e., ~10 to ~1 h;
- cycle life can be increased by a factor of three to four;
- the application of pulsed-current charging to a cycled battery (capacity = 80% initial value) can evoke a recovery in battery capacity;
- premature capacity loss occurs in both Pb–Sb and Pb–Ca–Sn cells at high rates of discharge with invariant-current charging;
- the capacity loss in Pb–Sb cells is governed by a progressive change in the state of the active material from low crystallinity in the precursor (initially charged) active material to well-defined crystallinity in the cycled mass; this, in turn, causes a decrease in both the specific surface area and the electrochemical reactivity with battery acid;
- the capacity loss in Pb–Ca–Sn cells is promoted both by a progressive crystallization of the active material during cycling and by the development of a barrier layer immediately adjacent to the grid member; the latter factor exerts the more dominant effect on capacity;
- any method that can slow down the crystallization process, as well as minimize the development and coverage of the barrier layer, will ameliorate premature capacity loss in both Pb–Sb and Pb–Ca–Sn batteries; it is found that pulsed-current charging techniques are an effective means for achieving these objectives.

Acknowledgements

The authors are grateful to Mr C.M. MacRae and Mr I.R. Harrowfield for assistance with the electron microprobe analysis.

References

[1] K. Kordesch, *J. Electrochem. Soc., 113* (1972) 1053.

[2] J.K. Nor, *EP Patent No. 0 311 460 A2* (Oct. 10, 1988); *US Patent No. 5 202 617* (Apr. 13, 1993).

[3] E.M. Valeriote, J.K. Nor and V.A. Ettel, *Proc. 5th Int. Lead/acid Battery Seminar,* International Lead Zinc Research Organization, Inc., Research Triangle Park, NC, USA, 1991, pp. 93–122.

[4] E.M. Valeriote and D.M. Jochim, *J. Power Sources, 40* (1992) 93.

[5] T.G. Chang, E.M. Valeriote and D.M. Jochim, *J. Power Sources, 48* (1994) 163.

[6] L.T. Lam, H. Ozgun, L.M.D. Cranswick and D.A.J. Rand, *J. Power Sources, 42* (1993) 55.

[7] E. Meissner and E. Voss, *J. Power Sources, 33* (1991) 231.

[8] R.J. Hill, A.M. Foxworthy and R.J. White, *J. Power Sources, 32* (1990) 315.

[9] C.G. Phyland, N.C. Wilson, I.R. Harrowfield, C.M. MacRae and A. Montgomery, *J. Comput. Assist. Microsc., 4* (1992) 271.

[10] A.F. Hollenkamp, K.K. Constanti, M.J. Koop, L. Apateanu, M. Calabek and K. Micka, *J. Power Sources, 48* (1994) 195.

[11] D.C. Constable, J.R. Gardner, K. Harris, R.J. Hill, D.A.J. Rand and L.B. Zalcman, *J. Electroanal. Chem., 168* (1984) 395.

[12] J. Yamashita and Y. Matsumaru, *J. Appl. Electrochem., 18* (1988) 595.

[13] D. Pavlov, *J. Power Sources, 46* (1993) 171.

[14] D.E. Swets, *J. Electrochem. Soc., 120* (1973) 925.

[15] A. Arifuku, H. Yoneyama and H. Tamura, *J. Appl. Electrochem., 11* (1981) 357.

[16] J.L. Dawson, M.I. Gillibrand and J. Wilkinson, in D.H. Collins (ed.), *Power Sources, 3,* Oriel, Newcastle upon Tyne, 1970, pp. 1–9.

[17] H.N. Cong, A. Ejjenne, J. Brenet and P. Faber, *J. Appl. Electrochem., 11* (1981) 373.

[18] J. Burbank, *J. Electrochem. Soc., 111* (1964) 765 and 1112.

[19] E.J. Ritchie and J. Burbank, *J. Electrochem. Soc., 117* (1970) 299.

[20] T.F. Sharpe, *J. Electrochem. Soc., 124* (1977) 168.

[21] M.K. Dimitrov and D. Pavlov, *J. Power Sources, 46* (1993) 203.

[22] D. Pavlov and N. Iordanov, *J. Electrochem. Soc., 117* (1970) 1103.

[23] P. Ruetschi, *J. Electrochem. Soc., 120* (1973) 331.

[24] B. Culpin, A.F. Hollenkamp and D.A.J. Rand, *J. Power Sources, 38* (1992) 63.